國 立 交 通 大 學

電子物理研究所

碩 士 論 文

碲化錳鋅磊晶層的高壓拉曼散射光譜研究

Raman scattering of $Zn_{1-x}Mn_xTe$ epilayers at high pressure

研 究 生：戴進吉

指導教授：周武清　教授

中華民國九十六年七月

碲化錳鋅磊晶層的高壓拉曼散射光譜研究

Raman scattering of $Zn_{1-x}Mn_xTe$ epilayers at high pressure

研 究 生：戴進吉　　Student：Jin-Ji Dai

指導教授：周武清 教授　　Advisor：Prof. Wu-Ching Chou

A Thesis
Submitted to Institute of Electrophysics
College of Science
National Chiao Tung University
in partial Fulfillment of the Requirements
for the Degree of Master
in
Electrophysics
July 2007
Hsinchu, Taiwan, Republic of China

中華民國九十六年七月

碲化錳鋅磊晶層的高壓拉曼散色光譜研究

研究生：戴進吉　　指導教授：周武清 博士

國立交通大學電子物理研究所

中文摘要

我們利用高壓拉曼散射光譜技術來研究參雜不同錳濃度的碲化錳鋅磊晶層，主要探討樣品的聲子頻率與壓力變化的關係。我們發現在高壓下半導體相變成為金屬會伴隨著縱向光學聲子模消失。我們以線性方程式去擬合閃鋅礦結構的聲子頻率與壓力的關係，得到相關的格留乃森(Grüneisen)參數和離子性，隨壓力增加離子性將會減少造成橫向聲子頻率接近縱向聲子頻率。除此之外，我們發現半導體到金屬相變壓力會隨著錳的濃度增加而減少。

Raman scattering of $Zn_{1-x}Mn_xTe$ epilayers at high pressure

Student：Jin-Ji Dai **Advisor：Dr. Wu-Ching Chou**

Institute of Electrophysics

National Chiao Tung University

Abstract

The pressure dependence of the optical phonon modes of cubic $Zn_{1-x}Mn_xTe$ ($0 \leqq x \leqq 0.22$) epilayers was investigated by using high-pressure Raman scattering technique. The pressure-induced metallization of zinc-blende (ZB) $Zn_{1-x}Mn_xTe$ together with the disappearance of the longitudinal optical (LO) phonon is observed. The measured phonon frequencies in the ZB phase region are fitted linearly. The Grüneisen parameters of the LO and transverse optical (TO) phonons are calculated. Additionally, the ionicity of the $Zn_{1-x}Mn_xTe$ layers is discussed. The frequency of TO phonon approaches the LO phonon as the pressure increases due to the decreasing of ionicity. The critical pressure in GPa of semiconductor-to-metal phase transition is found to decrease with the Mn fraction (x) as a function of $Pt = 11.5 - 28.7x - 54.5x^2$.

Acknowledgement

兩年的碩士生涯即將結束，我學會了思考問題與克服壓力，用心對待每一件事情，通常問題都能迎刃而解，當然不可否認的，交大土地公也幫了我很多忙。對於未來的工作相信會面臨更多的挑戰，要學習的實在太多了，然而學習中才會更了解自己，能讓自己進步與成長。

這篇論文能夠完成，我由衷的感謝指導教授周武清老師的支持與教導，提供我良好的實驗環境研究，在我錯誤及迷惘的時候，指引我正確的思考方向，不管在學術研究或待人處事上我都成長許多;也特別感謝李明知老師、陳衛國老師及張文豪老師於 meeting 時的寶貴意見，讓我在研究的過程懂得更嚴謹與細心。

對於實驗室的學長姐：謝博、祝壽、郭博、慶順、文政、李寧、京玉、繼祖、瑞雯、彥丞、阿邦、怡仁、文哲、狗哥、龜泰、維偲、啟仁、尚樺、阿許、聲嵩、泰鑫、士傑、士凱、老包等，謝謝你們的陪伴、教導與鼓勵，使我能順利畢業；在研究的過程中，先感謝阿邦學長帶領我學習及研究，是我的啟蒙學長，而我的麻吉京玉學長，真是辛苦你了，希望你能早一點畢業，除了陪你的小胖兒子，也要多陪老婆，然後生個小胖妹，最後我特別的感謝彥成學長在我最需要幫助的時候出現，你的支持鼓勵及實驗上的幫助，讓我研究上的瓶頸一一突破，沒有你就沒有這本論文的產生。而我的實驗夥伴筱筑、佩雯、少甫、書鴻、仲葳、峰毅，謝謝你們給予我的歡樂，其中特別感謝筱筑跟佩雯這兩位飯友，跟你們聊是非談八卦總是能忘記煩惱，希望你們能找到好工作、好男人。還有復凱、鏡學這兩位可愛的學弟，有你們的加入讓實驗室更加的歡樂，希望你們研究順利、早日畢業，就如鏡學說的~不要成為阿吉第二。

最後，我要感謝我最重要且親愛的家人及喬儀，特別是媽媽總是默默的辛勞付出，這二十年來妳辛苦了，我的成就是屬於妳的，而喬儀總是一直體貼我、鼓勵我，讓我度過許多的困境，母親跟喬儀是我一生中最重要的兩個女人，我完成此論文之喜悅將與你們分享。

Index

Chapter 1 Introduction

The high-pressure technique is a powerful experimental method for tuning the electronic energy bands and crystal structures of semiconductors. Hence, the physical properties of semiconductors at high pressure have attracted much attention that includes phase transition, phonon mode, energy gap, electron/hole density, and resistance, etc. Besides, the application of hydrostatic pressure has been successfully used in studies of mechanisms of lasing as well as in tuning of semiconductor laser diodes (LDs) [1,2]. Recently, ZnMnTe has attracted attention for future applications in LD [3] and solar cell [4]. However, the physical properties at high pressure of $Zn_{1-x}Mn_xTe$ still remain unexplored.

In our previous studies, the physical properties of ZnSe [5] and ZnSe-based ternary compounds, $Zn_{1-x}Fe_xSe$ [5], $Zn_{1-x}Mn_xSe$ [6], $ZnSe_{1-x}Te_x$ [7], and $Zn_{1-x}Cd_xSe$ [8], were investigated at high pressure. We observed that the LO phonon disappears at a critical pressure. It is an evidence of semiconductor-to-metal phase transition. During past several decades, various kind of high pressure studies on phase transition of ZnTe have been performed. The pressure-dependent energy band shift of ZnTe was investigated by an optical-absorption measurement [9]. A hexagonal cinnabar structure of ZnTe

was found between the ZB and metal structure by using a combined x-ray-absorption and diffraction spectroscopy study [10]. The phase transition from ZB to cinnabar and from cinnabar to orthorhombic *Cmcm* phases were identified by using x-ray diffraction experiment [11]. Furthermore, the change of the resistance with the applied pressure done by Shchennikov *et al*. offers powerful evidence that ZnTe exhibits pressure-induced metallization [12]. The above results show that the phase transition from ZB to cinnabar is at around 9.0 ± 0.5 GPa and the phase transition from cinnabar to *Cmcm* is at about 11.5 ± 0.5 GPa. However, according to the high-pressure Raman scattering measurement performed by Camacho *et al.*, the cinnabar phase transition together with the disappearance of the LO phonon occurs at around 10.0 GPa. The phase transition for cinnabar to *Cmcm* was also found at 14.2 GPa [13]. Moreover, Camacho *et al*. indicated that there exists a new phase between the transition regime from cinnabar to *Cmcm* (12.6 ~ 13.4 GPa). Their findings do not agree with the experimental results of x-ray [10,11], absorption [9], resistance [12], and theoretical calculation [14]. Consequently, in this work, high-pressure Raman scattering measurements was used to verify the pressure-induced phase transition in ZnTe epilayer. In addition, the phase transition and the crystal stability of ternary compounds $Zn_{1-x}Mn_xTe$ epilayer

with different Mn concentration under hydrostatic pressure will be explored.

In this thesis, the Raman spectra of ZB $Zn_{1-x}Mn_xTe$ ($0 \leqq x \leqq 0.22$) epilayers under hydrostatic pressure were studied at room temperature. The Mn concentration dependence of resonant Raman scattering (RRS) effect, phase transition pressure, Grüneisen parameter (γ_i), and the ionization of the $Zn_{1-x}Mn_xTe$ epilayers will be determined. Additionally, the critical pressure (Pt) of semiconductor-to-metal phase transition as a function of Mn content (x) will be presented.

Chapter 2 Experiment

In this chapter, we will introduce the experimental setup and the techniques that were used in our study. The experimental methods include high pressure technique and Raman scattering spectroscopy.

2.1 High-pressure Technique

2.1.1 Diamond Anvil Cell

The high pressure environment is generated by the diamond anvil cell (DAC). The schematic illustration of the DAC, which is a convenient tool for optical measurements, is shown in Fig. 2-1. The principle of all high-pressure cells can be described as follows. A force ***F*** is applied to a small surface area (*S*), creating a pressure ***P*** = ***F*** / ***S***. One can produce ultra-high pressure by reducing the size of the surface area (culet) of diamonds. The DAC is a convenient and easy tool to operate. The sample which is placed between two brilliant-cut diamonds is put into a thin metallic foil (gasket). As the applied force pushes the two opposite anvils together, the two opposite diamond anvils are compressed to

each other, producing high pressure environment. The culets are separated by a thin gasket, which was predrilled with a circular hole (sample chamber) by using an electrical discharge machine. The culets of the diamonds are all 500 μm. The thickness of the gasket is about 0.3 ~ 0.2 mm. The sample chamber is around 170 μm in diameter. After the sample is loaded into sample room, a drop of pressure-transmitting medium is filled to ensure hydrostatic conditions.

In the Fig. 2-1, “A” is the hemisphere rockers on which the diamond anvil was mounted; “B” is diamond; “C” is a gasket. A spring lever-arm is employed to generate force on the diamond surfaces. Force is applied through the lever-arm by turning the screws, which make the two opposite diamonds pressing mutually. Therefore, a hydrostatic and continuous varying pressure conditions are obtained.

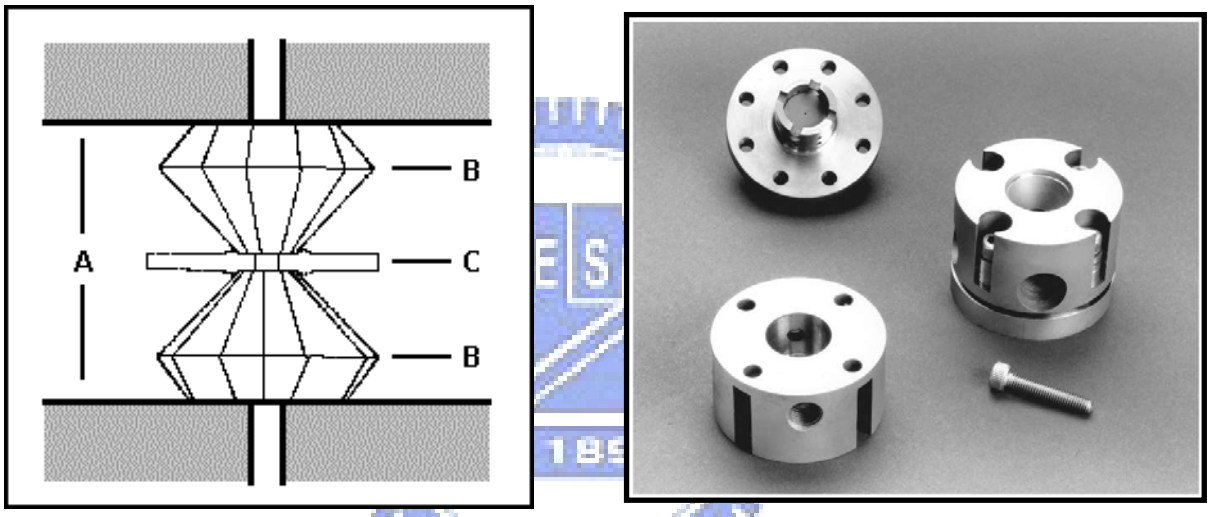

Fig. 2-1 Basic setup of diamond anvil cell.

2.1.2 Pressure Medium

To obtain a hydrostatic pressure environment within the sample chamber, a pressure medium is required. Traditionally, water is considered as a bad pressure medium because it transfers to solid ice VI and VII at 0.6 and 2.1GPa, respectively. The 4:1 methanol-ethanol mixed liquid as a pressure-transmitting medium, which is widely used in high-pressure measurements, is used in our experiments. The hydrostatic pressure was determined by the spectral shift of the ruby R1 line. The R1-R2 splitting in the ruby fluorescence was maintained well up to 25.4 GPa as shown in Fig. 2-2.

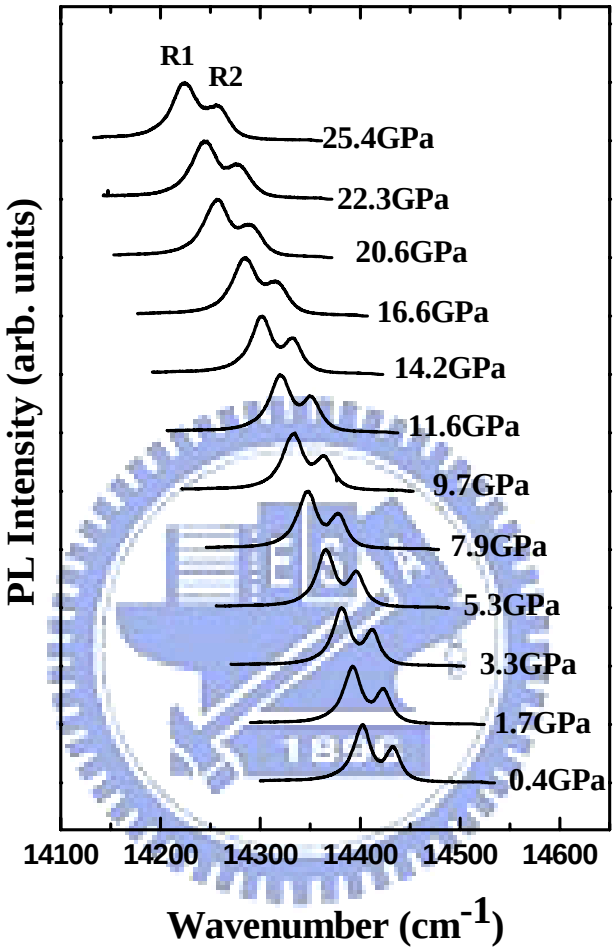

Fig. 2-2 Ruby fluorescence obtained by using pressure medium of 4:1 methanol-ethanol mixed liquid verse applied pressure. The right - hand and left - hand side peaks of the plots present R1 and R2 peaks of the ruby fluorescence lines, respectively.

2.1.3 Pressure Calibration

Various methods of pressure calibration involving the DAC have been used. Pressure in the DAC was estimated by calculating force over area, the known fixed point and the internal markers such as NaCl or silver in high-pressure X-ray studies. These methods are not convenient and are often proved to be inaccurate.

In 1972, the calibration of pressure in the DAC was overcome and became the most convenient method later. This breakthrough was successful because of the use of visual microscopic studies in the DAC. Foreman *et al.* first calibrated the shift of the R-line ruby fluorescence peaks as a function of pressure in the DAC, and demonstrated that this shift could be used as a convenient internal pressure calibration [15]. The technique incorporates a ruby crystal with the sample of interest and measures the pressure dependence of the sharp ruby R1 line fluorescence. The R-line of Cr^{+3}-doped Al_2O_3 shifts linearly to long wavelength with hydrostatic pressure in the range of 0.1 – 22.0 GPa. The R-line broadens if the ruby experiences non-hydrostatic stresses. A tiny ruby chip of 5-10 μm along with the sample in the pressure medium is excited by an Ar-ion laser. Figure 2-3 shows the energy levels and the resulting absorption and

luminescence for Cr^{+3} ions in ruby [16].

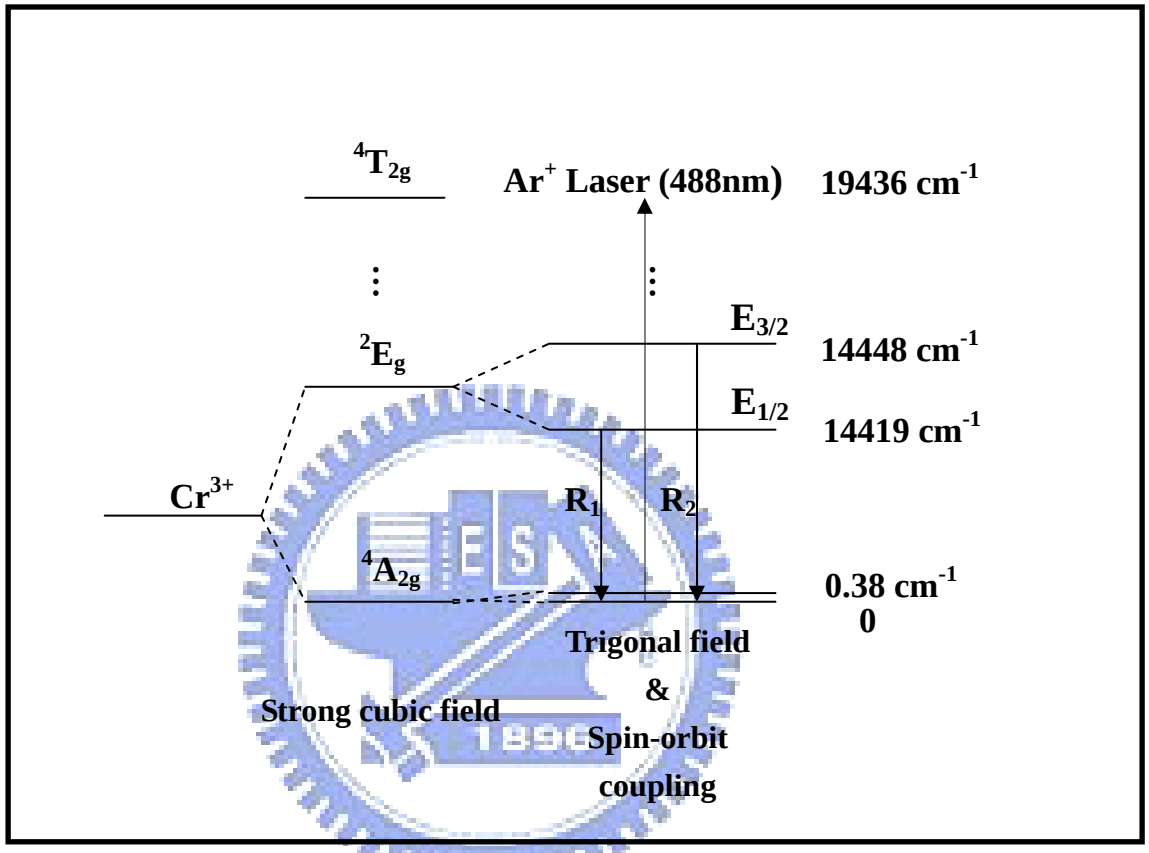

Fig. 2-3 Energy level of Cr^{+3}. The transitions of $E_{1/2} \rightarrow A$ and $E_{3/2} \rightarrow A$ give rise to R1 and R2 lines, respectively.

2.2 Micro-Raman Scattering Experiments

2.2.1 The Principle of Raman Scattering

In 1928, C. V. Raman, Indian physicist, first observed the inelastic scattering phenomenon of light in materials. When light encounters the surface of a semiconductor, most part of the light will be elastically scattered (Rayleigh scattering). There is no change in photon frequency during these elastic interactions. However, a small fraction of the light interact inelastically with phonon modes, producing outgoing photons whose frequencies are shifted from the incoming ones. This interaction of incident light with optical phonons called Raman scattering. When the polarization of optical phonon is transverse (longitudinal) relative to their wavevector of photon, it is call TO (LO) mode. The photon loses energy by emitting a phonon (Stokes shifted) or gains energy by absorbing a phonon (anti-Stokes shifted). The law of conservation energy and momentum must be applied in the process. The conservation conditions can be written as

$$h\nu_s = h\nu_i \pm h\nu_0 , \qquad (2.1)$$

$$k_s = k_i \pm k_0 . \qquad (2.2)$$

Where ν_i and ν_s are the incoming and scattered photon frequencies, respectively, k_i and k_s are the incoming and scattered photon wavevector, respectively, while ν_0 and k_0 are the phonon frequency and wavevector, respectively. The intensity of the anti-Stokes modes is normally much weaker than that of the Stokes modes. Raman scattering is inherently a weak process, but lasers provide enough power such that the spectra can be routinely measured [17].

All the Raman parameters – frequency and intensity, line shape and linewidth, polarization behavior – can be used to characterize the lattice, impurities, and free carriers in a semiconductor. The intensity gives information about the crystalline conditions. The linewidths increase when a material is damaged or disordered, because these conditions increase the phonon damping or break the momentum conservation during the Raman scattering process. The frequencies of the phonons can be used to determine the degree of alloying in a ternary material [18].

2.2.2 Experimental Setup

In Fig. 2-4, the schematic diagram of the Raman scattering experiment is shown. In this work, the Raman scattering measurements were performed by a Jobin-Yvon micro-Raman system. The Raman spectra were collected in backscattering configuration and at room temperature by using the 488 nm line of an Ar^+-ion laser as excitation. The intensity of Raman lines were normalized to the laser power as measured by a power meter. Usually, a laser beam with a power of 30 mW was focused to a size of ~ 5 μm on the sample surface in the DAC. To exclude the Reyleigh scattering, the 488 nm holographic notch plus filter was used to filter out the Reyleigh scattering of the laser. The spectra were analyzed by a SPEX 1404 double grating spectrometer equipped with a multichannel LN_2-cooled charge-coupled device (CCD). Finally, the spectrometer was controlled by a computer, which was used to store and plot the collected data.

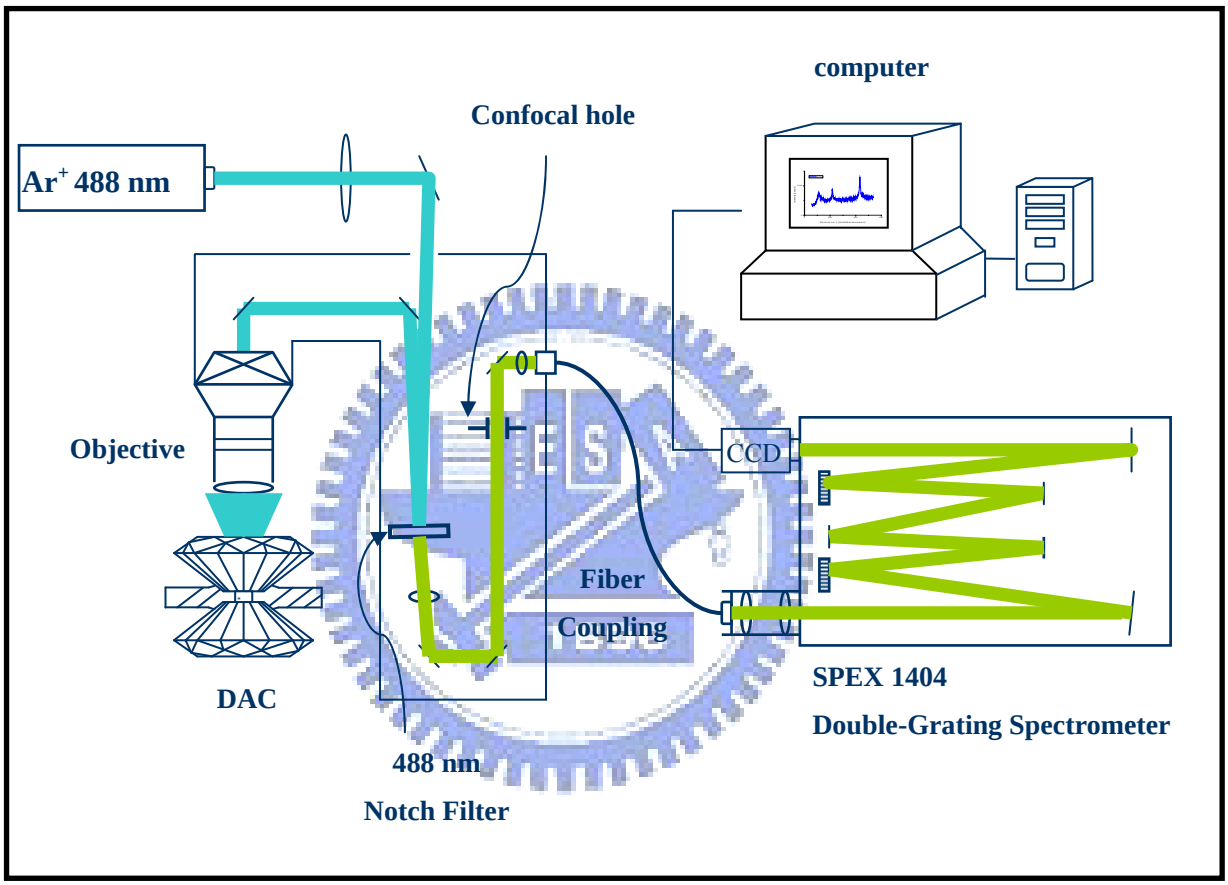

Fig. 2-4 Schematic diagram of micro-Raman system

2.3 Experimental Process

The $Zn_{1-x}Mn_xTe$ epilayers grown by MBE were loaded into the DAC. Prior to loading into diamond cells, the GaAs substrate was removed by mechanical polishing and chemical etching with H_2O : H_2O_2 : NaOH = 30 ml : 21 ml : 6 g mixture. The sample chamber was a circular hole with a diameter of ~ 170 μm and 100 μm thick, which was pre-drilled by using an electrical discharge machine. A methanol-ethanol 4:1 mixed liquid was used as a pressure-transmitting medium in order to maintain the hydrostatic conditions. In order to obtain hydrostatic conditions, the $Zn_{1-x}Mn_xTe$ epilayer and ruby chip (about 1μm in size) were sealed with the pressure transmitting medium in the sample chamber. The hydrostatic pressure was determined by measuring the spectral peak shift of the ruby R1-line fluorescence. The pressure gradient was less than 0.5 GPa, as determined by measurements made at various positions of the sample chamber.

Chapter 3 Results and Discussion

In this chapter, the lattice vibration of $Zn_{1-x}Mn_xTe$ epilayers with different Mn concentration will be studied by using Raman scattering measurement. All of the Raman spectra, discussed in section 3.1, were obtained at room temperature and under ambient pressure.

3.1 Raman scattering of $Zn_{1-x}Mn_xTe$ epilayers at atmospheric pressure

In Fig. 3-1, all the Raman spectra were measured under $z(x+y,x+y)\bar{z}$ backscattering geometry. We were not able to measure the TO mode because the Raman selection rule for this geometry is not allowed. As Mn content (x) increases, a weak impurity feature (I) attributed to the Mn atom in ZnMnTe epilayers is discovered. Therefore, two Raman modes, LO and I of $Zn_{1-x}Mn_xTe$ (x=0, 0.09, 0.14 and 0.22) epilayers were shown. The LO phonon of $Zn_{1-x}Mn_xTe$ epilayers appears at 204.2, 207.0, 207.8 and 209.4 cm^{-1} for x = 0.00, 0.09, 0.14, and 0.22, respectively. The blue-shift of LO phonon implies that the mass of the substituted element content (Mn) is less than Zn. The feature of I phonon appears at 192.6, 191.7 and 189.1 cm^{-1} for x = 0.09, 0.14, and 0.22 samples, respectively. Fig. 3-2 shows the frequency dependent LO and I phonon as a

function of Mn concentration (x). The solid square and solid circle denote the LO and *I* mode, respectively. As Mn content increases, the LO phonon shifts to higher frequency and the *I* mode shifts to lower frequency. This behavior agrees with the observation of the zone-center optical phonon mode of $Zn_{1-x}Mn_xTe$ bulks presented by Peterson *et al*. [19]. In addition, the impurity mode (*I*) is invisible for ZnTe (x = 0) epilayer.

3.2 Raman scattering of $Zn_{1-x}Mn_xTe$ epilayers at high pressure

In this section, the lattice vibrations and the semiconductor-to-metal phase transition of $Zn_{1-x}Mn_xTe$ ($0 \leq x \leq 0.22$) epilayers are studied by Raman scattering experiments at room temperature and under high pressures. The high pressure was generated by using the diamond anvil cell (DAC). The lattice constant and crystal volume of the ZnMnTe crystals were reduced by the applied pressure. As the applied pressure increases, the total energy of the crystal increases and makes the crystal unstable. Therefore, if there exists a new phase with lower energy, the crystal would release the energy and tend to have a phase change from unstable to stable condition.

The up-stroke pressure-dependent Raman spectra of $Zn_{1-x}Mn_xTe$ epilayers for x=0.00, 0.09, and 0.14 are respectively shown in Fig. 3-3, 3-4, and 3-5. As can be seen in Fig. 3-3, the frequency of both LO and TO phonon increase with applied pressure; however, the intensity of LO phonons do not monotonously

decline. The blue-shift of phonon frequency implies the shortening of lattice constant, in other words, the crystal becomes harder. The peak intensity of LO phonon does not monotonously decline because of the resonant Raman scattering (RRS) effect. According to the RRS condition, while the incident laser energy is sufficiently close to the energy of the electronic transition, the pressure-driven RRS effect occurs [8,20].

$$E_{laser} - mhv_{LO}(p) = E_{exc}(p), \quad (3.1)$$

Where E_{laser} is the photon energy of the incident laser, $hv_{LO}(p)$ is the pressure dependence energy of the LO phonon, m is the overtone order of LO phonons, $E_{laser} - hv_{LO}(p)$ is the pressure-dependence LO Raman energy, and $E_{exc}(p)$ is the pressure-dependence exciton energy. The band gap of $Zn_{1-x}Mn_xTe$ epilayers was usually controlled by tuning the Mn concentration during the growth, or manipulating the pressure and temperature of the sample chamber. In this investigation, the band gap of $Zn_{1-x}Mn_xTe$ epilayers shifts with Mn content (x) and applied pressure, but the incident laser energy was fixed at 2.54 eV with an Ar-ion 488 nm laser.

In Fig. 3-3, for ZnTe epilayers at room temperature, as the external pressure was gradually tuned toward 3.7 GPa, the exciton energy of ZnTe approached the laser energy and an increase in intensity of LO phonon was

observed. By further increasing the pressure to around 4.4 GPa, the exciton energy of ZnTe exceeds the incident laser energy and begins to move away from the RRS condition. Therefore, the intensity of LO phonon decreases monotonously with the increasing pressure. At around 11.5 GPa, the LO phonon disappears and the sample becomes opaque, which is attributed to the semiconductor-to-metal phase transition [5,6,7,8]. Because the semiconductor becomes metal, the excitation laser beam is not allowed to penetrate into the sample. Additionally, the disappearance of LO phonon is the evidence of the phase transition from the semiconductor to the metal phase. Furthermore, above 3.7 GPa, under the RRS condition, the TO phonon mode becomes pronounced. Under 8.7 GPa, the TO and LO phonons shift to higher frequencies with pressure. Nevertheless, as the pressure is raised to around 8.7 GPa, a split TO phonon mode begins to appear. As the pressure is increased further, the split TO phonon shifts toward lower frequency. This behavior implies that the lattice in the direction becomes soft [21]. The splitting of the TO mode in the up-stroke process also implies the formation of the cinnabar phase, which results from the lowering of the crystal symmetry [5,6,7,22]. However, at about 11.5 GPa, the Raman spectra still exhibit the TO mode when the semiconductor becomes metal. It can be ascribed to the fact that transverse surface lattice vibrations are allowed in both semiconductor and metal, even if the skin depth (or penetration depth) of the metal into which the laser penetrates is merely several tens of angstroms [5,8]. Similar experimental results were obtained in earlier

investigations of ZnSe-based ternary compounds.

The disappearance of LO phonon in the up-stroke process at about 11.5 ± 0.2 GPa, implying that the semiconductor-to-metal phase transition occurred. Similarly, Strössner *et al*. found that the phase transition from semiconductor to metal phase in ZnTe is at around 11.9 ± 0.3 GPa by using optical-absorption measurement [9]. San-Miguel *et al.* found that the cinnabar and the metallic phase transition of ZnTe respectively appeares at around 9.5 ± 0.5 GPa and 12 ± 0.5 GPa by using x-ray-absorption and -diffraction spectroscopy [10]. Furthermore, using x-ray diffraction measurement, Nelmes *et al*. determined that the metallic phase observed at around 11.5 GPa is an orthorhombic *Cmcm* structure. The structure transition from ZB to cinnabar occurs at around 8.9 GPa [11]. Recently, the pressure-dependent resistance measurement of ZnTe crystal was performed by Shchennikov *et al*. As the applied pressure increases, the resistance drops abruptly and then slightly increases at around 9.0 GPa. The behavior is attributed to the phase transition from ZB to cinnabar. At around 12.0 GPa, the resistance drastically decreases again by nearly 6 orders of magnitude. Shchennikov *et al*. assign this behavior to the phase transition from cinnabar to orthorhombic *Cmcm*. The abrupt decrease of the resistance at about 12.0 GPa is also an evidence of pressure-induced metallization [12].

However, the high-pressure Raman scattering study of ZnTe performed by Camacho *et al.* [13], asserts that the cinnabar phase transition together with the disappearance of the LO phonon occurs at around 10.0 GPa. The phase

transition of cinnabar to *Cmcm* was also found at 14.2 GPa. Moreover, the authors also indicate that there exists a new phase between the transition regime from cinnabar to *Cmcm* (12.6 ~ 13.4 GPa). The phase transition pressure, the disappearance of the LO phonon due to the occurrence of the cinnabar phase, and a new phase between the transition regime from cinnabar to *Cmcm* (12.6 ~ 13.4 GPa) observed by Camacho *et al.* conflict with our experimental results described above.

In Fig. 3-4 and 3-5, the up-stroke pressure dependence of the LO, TO, and *I* mode are shown for $Zn_{1-x}Mn_xTe$ (x = 0.09 and 0.14) epilayers. As the sample become metallic, the *I* mode is still visible. It could be due to the fact that the impurity mode is likely a surface vibration mode. By contrast, pressure-driven RRS effect and the pressure-induce phase transition are at different pressures. For x=0, the RRS effect occurs at around 4.0 GPa, and the TO phonon splitting transpires at around 8.7 GPa and the LO phonon disappears at around 11.5 GPa. For x = 0.09, the RRS effect occurs at around 3.0 GPa, and the TO phonon splitting transpires at around 6.7 GPa and the LO phonon disappears at around 9.3 GPa. For x = 0.14, the RRS effect occurs at around 2.5 GPa, and the TO phonon splitting transpires at around 5.3 GPa and the LO phonon disappears at around 8.6 GPa.

Fig. 3-6 displays the pressure dependence of the LO phonon intensity for $Zn_{1-x}Mn_xTe$ (x = 0, 0.09 and 0.14) epilayers. The maximum LO phonon intensity occurs at 4.0, 3.0 and 2.5 GPa for ZnTe, $Zn_{0.9}1Mn_{0.09}Te$ and

$Zn_{0.86}Mn_{0.14}Te$ epilayers, respectively. As the Mn content is increased, the pressure of RRS effect decreases, which results from the increasing of the exciton energy. In addition, the Fig. 3-7 gives the intensities of the LO phonon as a function of LO Raman energy for $Zn_{1-x}Mn_xTe$ (x = 0, 0.09 and 0.14) epilayers. As the LO Raman energy closes to about 2.513 eV, the RRS effect on LO phonon reaches the maximum.

Fig. 3-8 shows the decline in the pressure of the phase transition as a function of Mn content (x) for the $Zn_{1-x}Mn_xTe$. The solid lines represent a quadratic fit, given by $Pt = 11.5 - 28.7x - 54.5x^2$ in GPa. The critical pressure of semiconductor-to-metal phase transition (Pt) falls with increasing Mn content (x) because the crystal becomes unstable. The crystal becomes unstable as the substituted element increases. It has been also observed in ZnSe-based ternary semiconductors. For instance, C. S. Yang *et al.* found that the structural transition of $Zn_{1-x}Mn_xSe$ (x=0.07 and 0.24) from zinc-blende to rocksalt occurred at around 11.8 and 9.9 GPa, respectively. For $ZnSe_{1-x}Te_x$ ($0 \leqq x \leqq 0.54$) epilayers, the critical pressure of semiconductor-to-metal phase transition drops from 13.7 to 7.3 GPa [6,7]. Recently, Y. C. Lin *et al.* revealed that the semiconductor-to-metal phase transition pressure of $Zn_{1-x}Cd_xSe$ ($0 \leqq x \leqq 0.32$) epilayers falls from 13.6 to 9.4 GPa.

The pressure dependence of all the Raman mode frequencies of $Zn_{1-x}Mn_xTe$ (x = 0.00, 0.09, and 0.14) epilayers are shown in Fig. 3-9, 3-10, and 3-11,

respectively. The squares, circles and triangles represent the LO, I, and TO mode, respectively. The LO, I, and TO frequencies of $Zn_{1-x}Mn_xTe$ exhibit a blue-shift with applied pressure but the split TO mode exhibits red-shift. The arrows in Fig. 3-9, 3-10, and 3-11 denote the phase transition from ZB to cinnabar and cinnabar to *Cmcm*. The pressure-dependent LO and TO phonon frequency in the ZB phase region is fitted linearly. The solid lines are the fitting results, described by the following equations:

The fitting equations of ZnTe are expressed as follows:

$$\omega_{LO} = 204.2 + 3.48P \quad (3.2)$$

$$\omega_{TO} = 179.6 + 3.56P \quad (3.3)$$

The fitting equations of $Zn_{0.91}Mn_{0.09}Te$ are expressed as follows:

$$\omega_{LO} = 207.0 + 3.67P \quad (3.4)$$

$$\omega_{TO} = 177.5 + 4.23P \quad (3.5)$$

The fitting equations of $Zn_{0.86}Mn_{0.14}Te$ are expressed as follows:

$$\omega_{LO} = 207.8 + 3.91P \quad (3.6)$$

$$\omega_{TO} = 175.2 + 4.82P \quad (3.7)$$

Where ω is the phonon frequency of unit cm^{-1} and P is the pressure in GPa. The pressure-dependent phonon frequency (ω_i and $d\omega_i / dp$) and all of the fitting parameters are listed in Table. 3-1. In addition, the pressure dependence of the phonons response can be characterized in the term of dimensionless Grüneisen

parameter (γ_i), and is given by [23]

$$\gamma_{\mathrm{i}} = -\left(\frac{d\ln\omega_{\mathrm{i}}}{d\ln \mathrm{V}}\right) = \frac{1}{\beta}\frac{\partial \ln\omega_{\mathrm{i}}}{\partial p} = \left(\frac{K_0}{\omega_{\mathrm{i}}}\right)\left(\frac{d\omega_{\mathrm{i}}}{dp}\right) \quad , \tag{3.8}$$

where V is the molar volume in cm^3/mol and K_0 is the bulk modulus defined as the inverse of the isothermal volume compressibility (β). Because the bulk modulus (K_0) of ZB ZnMnTe is not available, the value of $K_{0\,(\mathrm{ZB\ ZnTe})} = 50.5$ is used [10]. In comparison with the Grüneisen parameter of all $Zn_{1-x}Mn_xTe$ epilayers, the behavior, $\gamma_{TO} > \gamma_{LO}$, is found. Also, as the Mn content increases, both γ_{LO} and γ_{TO} increase. In addition, the frequency difference of LO and TO phonons ($\omega_{\mathrm{LO}} - \omega_{\mathrm{TO}}$) are found to increase with Mn content. However, the frequency difference ($\omega_{\mathrm{LO}} - \omega_{\mathrm{TO}}$) is observed to fall with applied pressure for all $Zn_{1-x}Mn_xTe$ samples. It is due to the fact that the pressure dependence of the frequency difference ($\omega_{\mathrm{LO}} - \omega_{\mathrm{TO}}$) can be related to the bond-length dependence of ionicity and polarity [24]. Consequently, the applied pressure tends to reduce the bond length and the ionicity of $Zn_{1-x}Mn_xTe$ crystal.

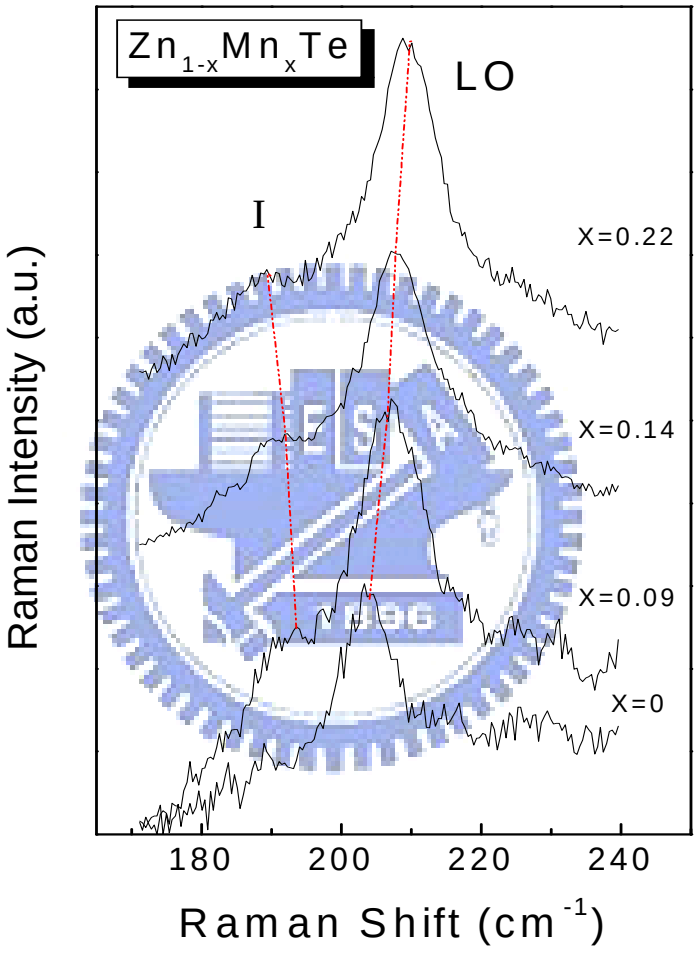

Fig. 3-1 Raman spectra of $Zn_{1-x}Mn_xTe$ for x = 0.00, 0.09, 0.14 and 0.22 at ambient pressure.

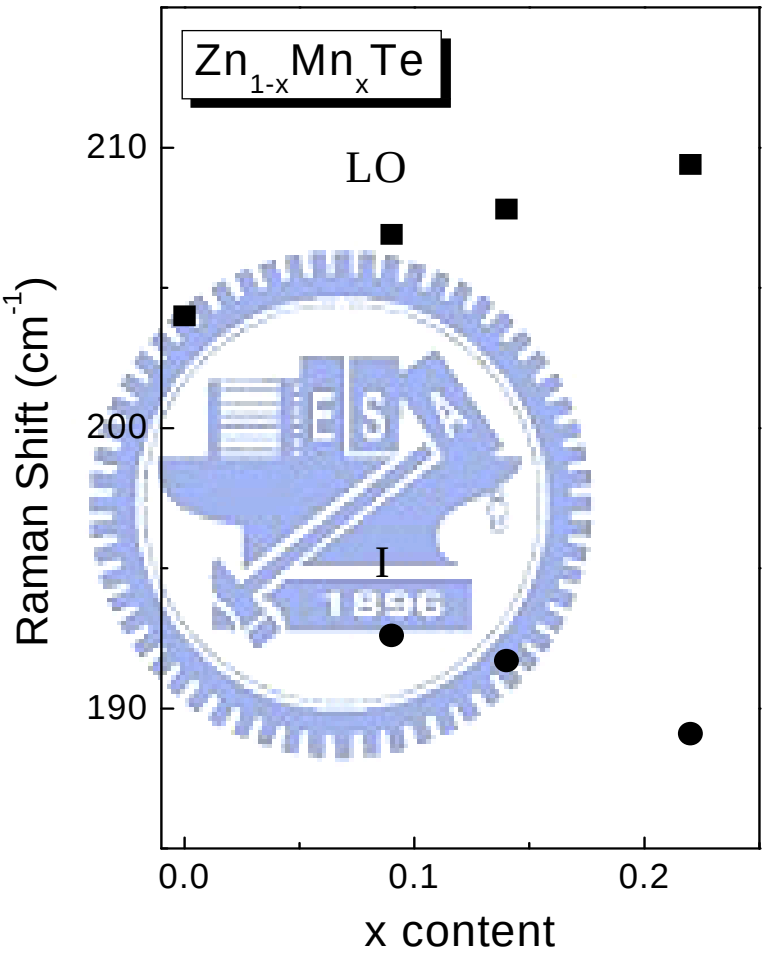

Fig. 3-2 Dependence of LO and *I* phonon frequency

as a function of the Mn concentration (*x*) in zinc-blende $Zn_{1-x}Mn_xTe$.

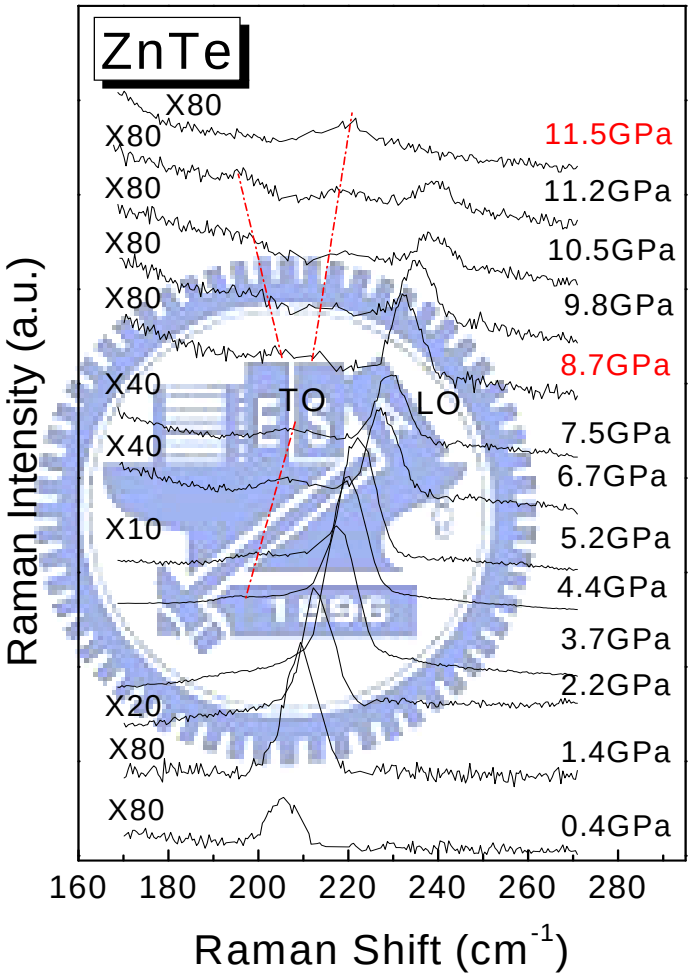

Fig. 3.3 Raman spectra of ZnTe at different pressure.

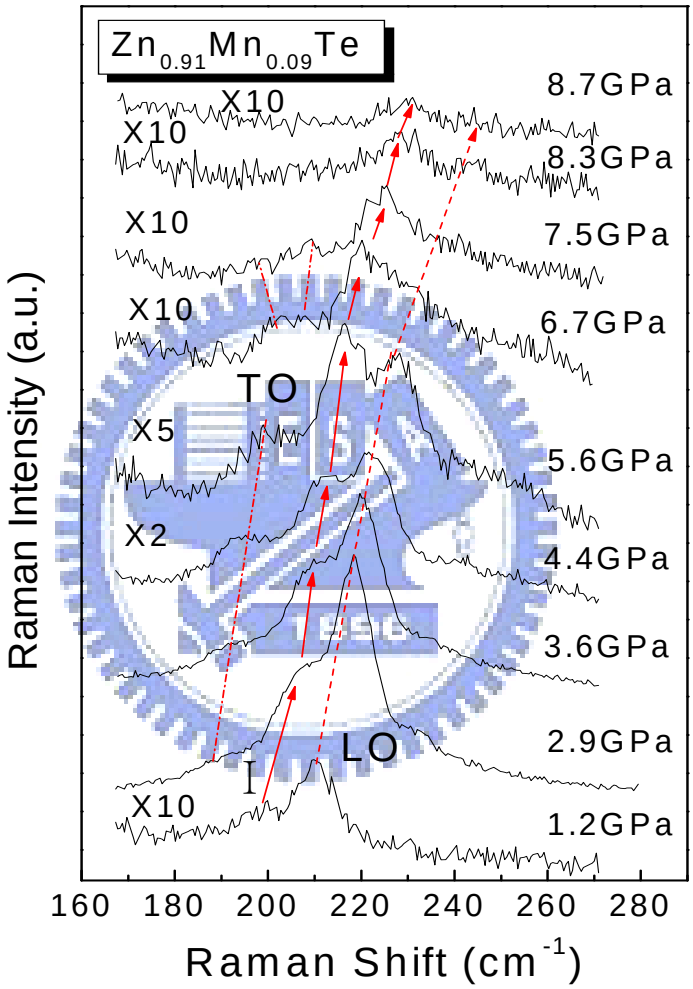

Fig. 3-4 Raman spectra of $Zn_{0.91}Mn_{0.09}Te$ at different pressure.

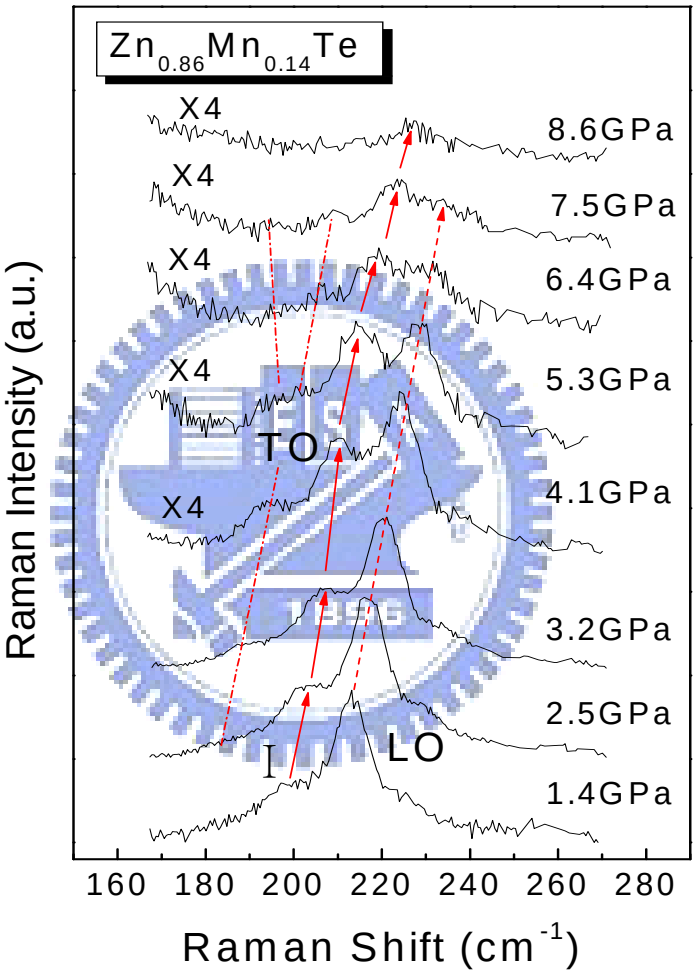

Fig. 3-5 Raman spectra of $Zn_{0.86}Mn_{0.14}Te$ at different pressure.

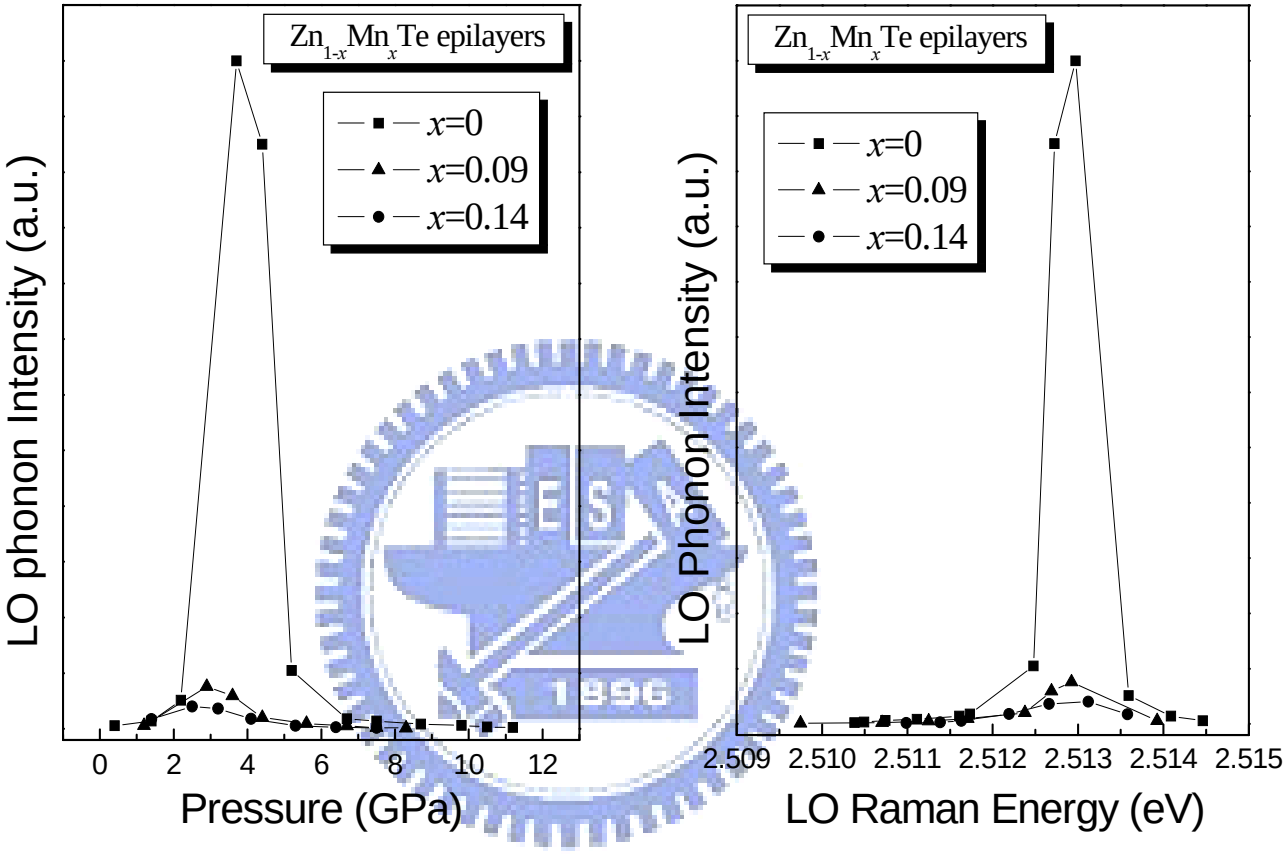

Fig. 3-6 Pressure dependence of LO phonon intensity for $Zn_{1-x}Mn_xTe$ (x = 0, 0.09 and 0.14) epilayers.

Fig. 3-7 Intensities of the LO phonon as a function of LO Raman energy for $Zn_{1-x}Mn_xTe$ (x = 0, 0.09 and 0.14) epilayers.

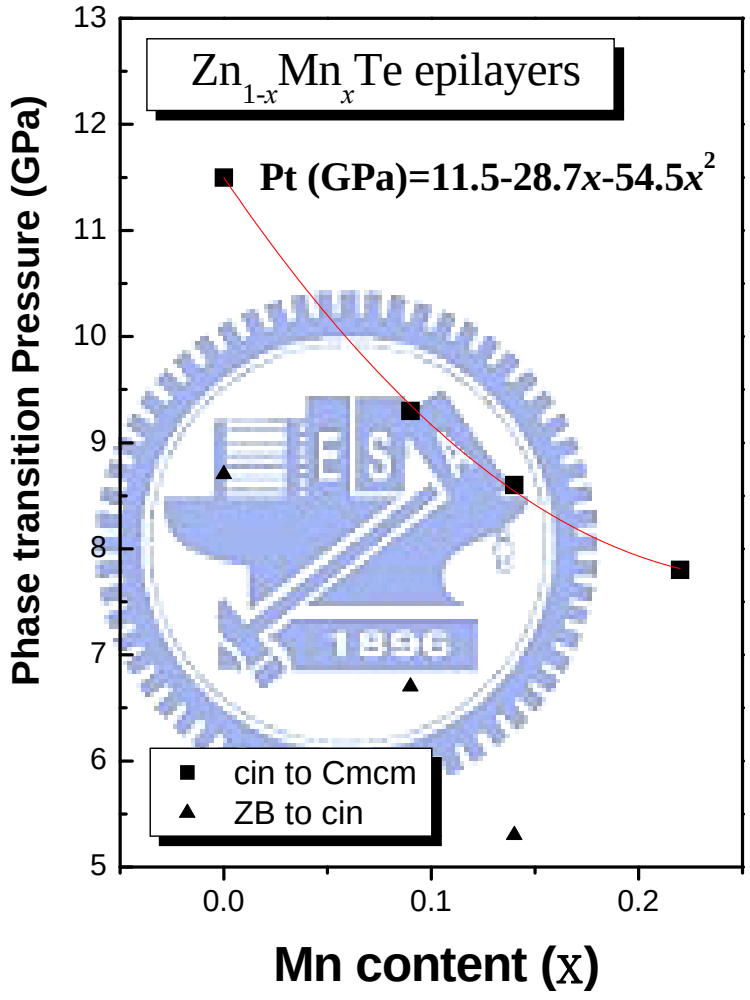

Fig. 3-8 Pressure of the phase transition as a function of Mn content (x) for the ZnMnTe.

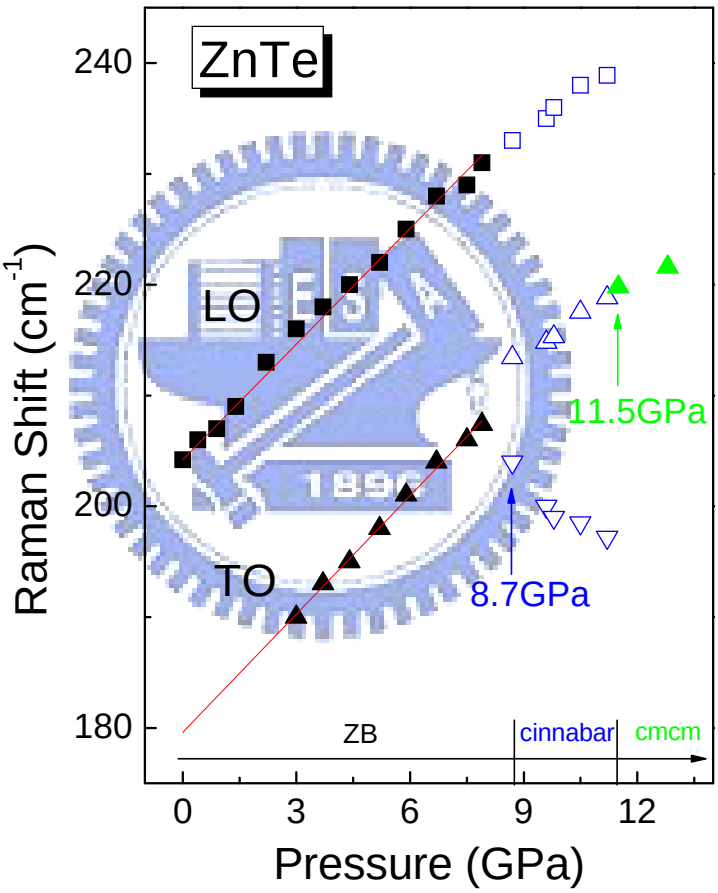

Fig. 3-9 Pressure dependence of LO and TO peak energies for ZnTe.

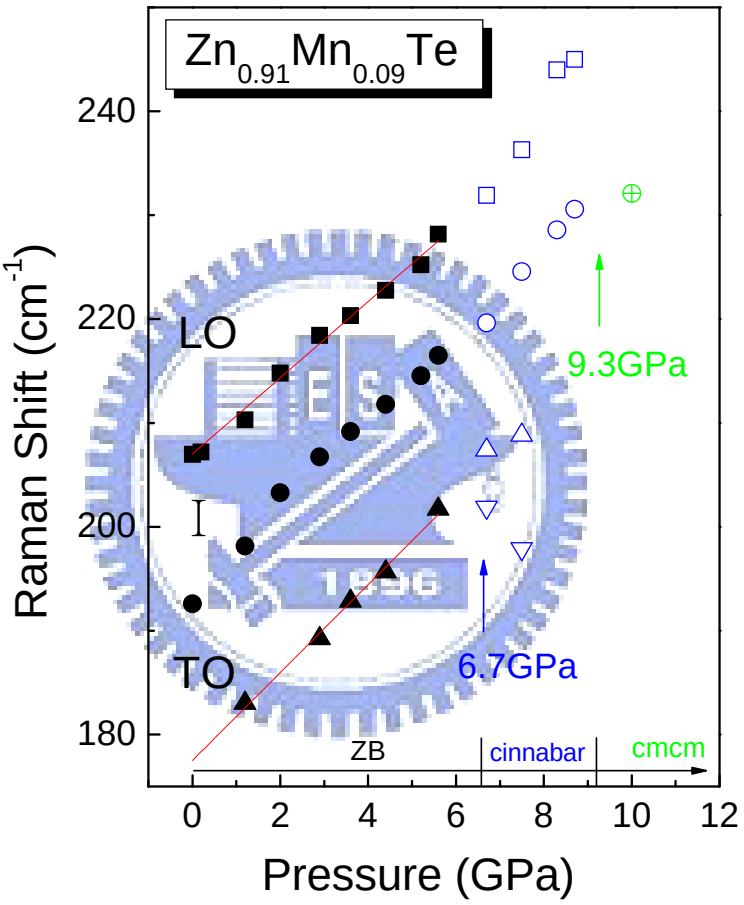

Fig. 3-10 Pressure dependence of LO, I, and TO peak energies for $Zn_{0.91}Mn_{0.09}Te$.

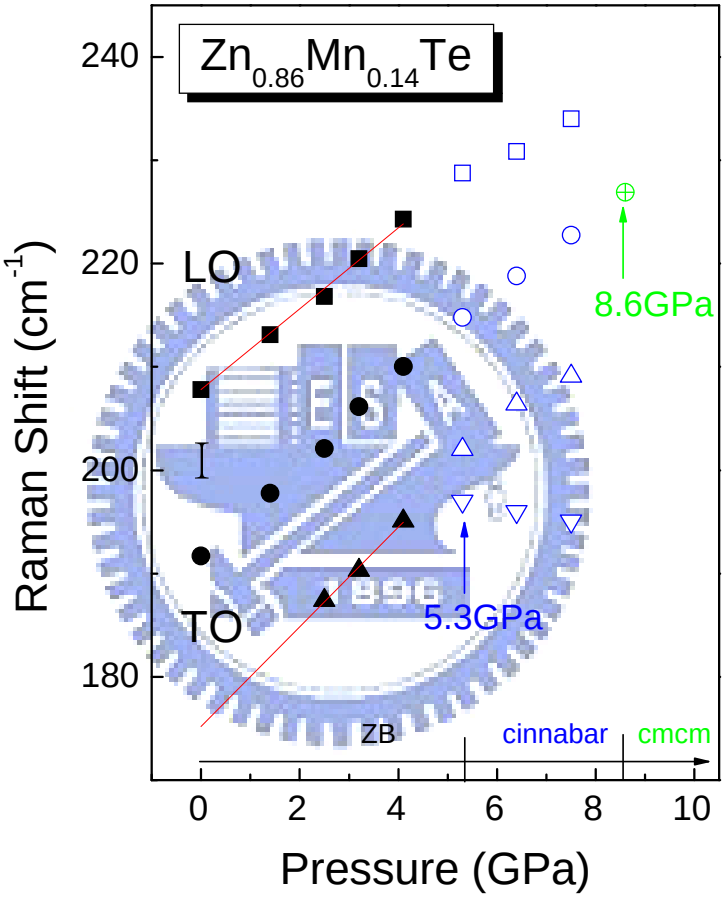

Fig. 3-11 Pressure dependence of LO, I, and TO peak energies for $Zn_{0.86}Mn_{0.14}Te$.

Sample	mode	(ZB) linear fitting ω_{LO} , ω_{LO}	ω_i (cm^{-1})	$d\omega_i/dp$ (cm^{-1}/GPa)	RRS (GPa)	transition Pressure (GPa)	γ_i	$\omega_{LO}-\omega_{TO}$ (ionicity)
ZnTe	LO	204.2 + 3.48P	204.4	3.48	~ 4.0	~11.5±0.2	0.86	24.6-0.08P
	TO	179.6 + 3.56P	179.6	3.56		~8.7±0.5	1.00	
$Zn_{0.91}Mn_{0.09}Te$	LO	207.0 + 3.67P	207.0	3.67	~ 3.0	~9.3±0.5	0.90	29.5-0.56P
	TO	177.5 + 4.23P	177.5	4.23		~6.7±0.5	1.20	
$Zn_{0.86}Mn_{0.14}Te$	LO	207.8 + 3.91P	207.8	3.91	~ 2.5	~8.6±0.5	0.95	32.6-0.91P
	TO	175.2 + 4.82P	175.2	4.82		~5.3±0.5	1.39	

Table.3-1 High-pressure dependence of phonon frequencies for $Zn_{1-x}Mn_xTe$ epilayers (ω_{LO}, ω_{TO}). The values of mode frequency (ω_i), pressure coefficient ($d\omega_i/dp$), Grüneisen parameter (γ_i), and ionicity were also listed.

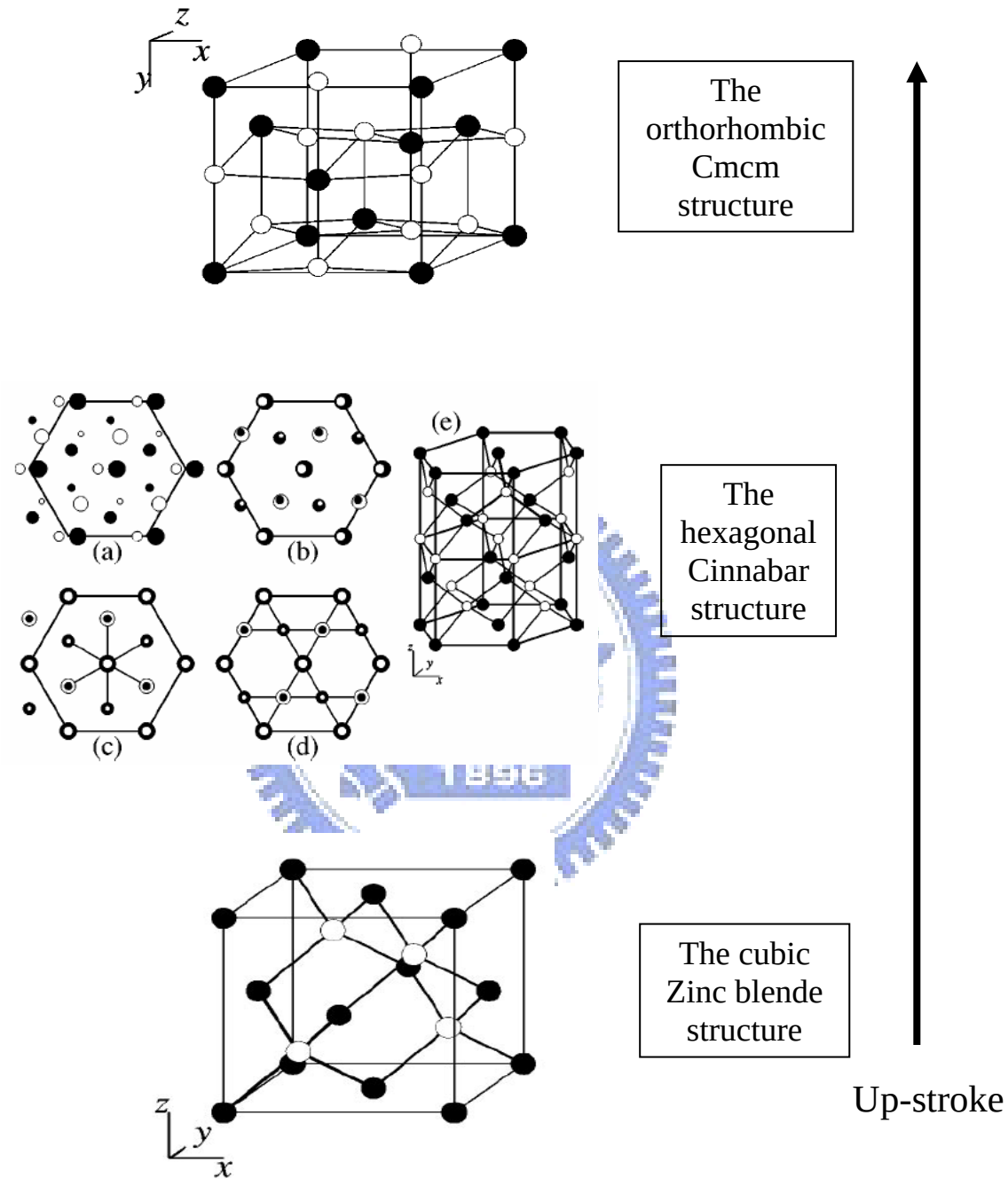

Fig. 3-12 Structures transition of $Zn_{1-x}Mn_xTe$ (x = 0, 0.09, 0.14)

in the up-stroke process.

Chapter 4 Conclusions

The zone-center optical phonon modes of $Zn_{1-x}Mn_xTe$ (x=0, 0.09, 0.14 and 0.22) epilayers were investigated by using high-pressure Raman scattering experiment. The pressure-driven RRS effect is observed in all the studied $Zn_{1-x}Mn_xTe$ samples. In the up-stroke pressurized process, the splitting of TO mode could be ascribed to the phase transition from ZB to *Cinnabar*. Moreover, the disappearance of the LO mode is an evidence of semiconductor to metal (*Cmcm* phase) phase transition. The pressure-dependent LO and TO phonon frequency in the ZB phase region are fitted linearly. The dimensionless Grüneisen parameter and LO-TO splitting are obtained. In comparison with the Grüneisen parameter of all $Zn_{1-x}Mn_xTe$ epilayers, the behavior of $\gamma_{TO} > \gamma_{LO}$ is found. Also, as the Mn content increases, both γ_{LO} and γ_{TO} increase. Of all the $Zn_{1-x}Mn_xTe$ layers, the frequencies of LO and TO phonon are getting closer to each other when the pressure is increased. This is because the applied pressure tends to reduce the bond length and the ionicity of $Zn_{1-x}Mn_xTe$ crystal. The semiconductor-to-metal phase transition pressure is found to decrease as the Mn concentration increases.

References

[1] T.Suski, G. Franssen, P. Perlin, R. Bohdan, A. Bercha, P. Adamiec, F. Dybala, W. Trzeciakowski, P. Prystawko, M. Leszczynski, I. Grzegory, and S. Porowski, Appl. Phys. Lett. **84**, 1236 (2004).

[2] P. Adamiec, A. Salhi, R. Bohdan, A. Bercha, F. Dybala, W. Trzeciakowski, Y. Rouillard, and A. Joullie, Appl. Phys. Lett. **85**, 4292 (2004).

[3] D. Raja Reddy and B. K. Reddy, Appl. Phys. Lett. **81**, 460 (2002).

[4] K. M. Yu, W. Walukiewicz, J. Wu, W. Shan, M. A. Scarpulla, O. D. Dubon, J. W. Beeman, and P. Becla, Phys. Stat. Sol. (b) **241**, 660 (2004).

[5] Chih-Ming Lin, Der-San Chuu, and Tzong-Jer Yang, Phys. Rev. B **55**, 13641 (1997).

[6] C. S. Yang, C. S. Ro, W. C. Chou, C. M. Lin, D. S. Chuu, J. Hu, E. Huang, and J. Xu, J. Appl. Phys. **85**, 8092 (1999).

[7] C. S. Yang, W. C. Chou, D. M. Chen, C. S. Ro, J. L. Shen, and T. R. Yang, Phys. Rev. B **59**, 8128 (1999).

[8] Y. C. Lin, C. H. Chiu, W. C. Fan, S. L. Yang, D. S. Chuu, and W. C. Chou, J. Appl. Phys. **101**, 073507 (2007).

[9] K. Strossner, S. Ves, Chul Koo Kim, and M. Cardona, Solid State

Commun. **61**, 275 (1987).

[10] A. San-Miguel, A. Polian, M. Gauthier, and J. P. Itie, Phys. Rev. B **48**, 8683 (1993).

[11] R. J. Nelmes, M. I. McMahon, N. G. Wright, and D. R. Allan, Phys. Rev. Lett. **73**, 1805 (1994).

[12] Vladimir V. Shchennikov, Sergey V. Ovsyannikov, Andrey Y. Derevskov, Vsevolod V. Shchennikov Jr, J. Phys. Chem. Solids **67**, 2203 (2006).

[13] J Camacho, I Loa, A Cantarero, and K Syassen, J. Phys: Condens. Matter **14**, 739 (2002).

[14] Gun-Do Lee and Jisoon Ihm, Phys. Rev. B **53**, R7622 (1996).

[15] R. A. Forman, G. J. Piermarini, J. D. Barnett, and S. Block, Science **176**, 284 (1972).

[16] E. Huang, J. Geol. Soc. China **32**, 924 (1992).

[17] I. F. Chang and S. S. Mitra, Phys. Rev. **172**, 924 (1968).

[18] A. Chergui, J. Valenta, and J. L. Loison, Semiconductor Science Technology **9**, 2073 (1994).

[19] D. L. Peterson, A. Petrou, W. Giriat, A. K. Ramdas, and S. Rodriguez, Phys. Rev. B **33**, 1160 (1986).

[20] W. S. Li, Z. X. Shen, D. Z. Shen, and X. W. Fan, J. Appl. Phys. **84**, 5198 (1998).

[21] Akhilesh K. Arora, E. K. Suh, U. Debska, and A. K. Ramdas, Phys.

Rev. B **37**, 2927 (1988).

[22] Akhilesh K. Arora, and T. Sakuntala, Phys. Rev. B **52**, 11052 (1995).

[23] M. Blackman and W. B. Daniels, in *Light Scattering in Solids IV*, edited by M. Cardona, and G. Güntherodt (Springer, Berlin, 1984), Chap. 8.

[24] P. Perlin, T. Suski, J. W. Ager III, G. Conti, A. Polian, N. E. Christensen, I. Gorczyca, I. Grzegory, E. R. Weber, and E. E. Haller, Phys. Rev. B **60**, 1480 (1999).